Annu. Rev. Biochem. 2001. 70:149–80

CHANNELING OF SUBSTRATES AND INTERMEDIATES IN ENZYME-CATALYZED REACTIONS

Xinyi Huang[1], Hazel M. Holden[2], and Frank M. Raushel[3]
[1]*Wyeth-Ayerst Research, 401 North Middleton Road, Pearl River, New York 10965; e-mail: huang@war.wyeth.com*
[2]*Department of Biochemistry, College of Agricultural and Life Sciences, University of Wisconsin, 433 Babcock Drive, Madison, Wisconsin 53706*
[3]*Department of Chemistry, Texas A&M University, College Station, Texas 77842-3012; e-mail: raushel@tamu.edu*

Key Words molecular tunnels, reaction intermediates

■ **Abstract** The three-dimensional structures of tryptophan synthase, carbamoyl phosphate synthetase, glutamine phosphoribosylpyrophosphate amidotransferase, and asparagine synthetase have revealed the relative locations of multiple active sites within these proteins. In all of these polyfunctional enzymes, a product formed from the catalytic reaction at one active site is a substrate for an enzymatic reaction at a distal active site. Reaction intermediates are translocated from one active site to the next through the participation of an intermolecular tunnel. The tunnel in tryptophan synthase is ∼25 Å in length, whereas the tunnel in carbamoyl phosphate synthetase is nearly 100 Å long. Kinetic studies have demonstrated that the individual reactions are coordinated through allosteric coupling of one active site with another. The participation of these molecular tunnels is thought to protect reactive intermediates from coming in contact with the external medium.

CONTENTS

INTRODUCTION

The channeling (or tunneling) of substrates is a mechanistic process for the direct delivery of a reaction intermediate (I) from the active site of one enzyme (E_1) to the active site of a second enzyme (E_2) without prior dissociation into the bulk solvent. Thus, the reaction products from one active site are actively or passively translocated directly to another active site as graphically illustrated in Scheme 1 (1–4). Channeling of this kind can theoretically occur within multifunctional enzymes, tightly associated multienzyme complexes, or transient enzyme complexes.

$$S \xrightarrow{E_1} [I] \xrightarrow{E_2} P$$

Substrate channeling has many advantages over the free diffusion of reaction products within the bulk solvent. The transit time for the movement of reaction products from one active site to the next is reduced (5, 6). Chemically labile intermediates can be protected from decomposition by the aqueous external environment (7). Unfavorable equilibria can be circumvented (8–10) and reaction intermediates can be segregated from competing enzymatic transformations. Examples of substrate channeling have been cited for numerous biochemical pathways (1, 11–17), including purine and pyrimidine biosynthesis, amino acid metabolism, lipid metabolism, glycolysis, the tricarboxylic acid cycle, DNA replication, RNA synthesis, and protein biosynthesis. However, direct and compelling experimental evidence for substrate channeling is lacking in many cases claimed for transient enzyme complexes and a large number of the proposed examples of metabolic channeling. As the concept of metabolic channeling has been recently discussed (1–3), this review instead focuses on several multifunctional enzymes and tightly associated multienzyme complexes for which a substantial body of biochemical and structural evidence is now available to support the idea of substrate channeling.

The tunneling of reaction intermediates in multifunctional enzymes and multienzyme complexes has been investigated by a variety of kinetic approaches, including the measurement of the transit time of reaction intermediates, isotope dilution of endogenous reaction intermediates, competing reactions, and transient-state kinetics. For example, if a reaction intermediate (I) is directly tunneled from one active site (E_1) to another (E_2) (Scheme 1), then the transit time will approach zero. However, if only some of the intermediate is transferred to the next active site (leaky channeling), then the experimental transit time will be less than that for a free diffusion mechanism, but it will not be zero. The method of isotope

dilution is illustrated in Scheme 2. With this protocol a large excess of unlabeled intermediate (I) competes with the endogenously generated isotopically labeled intermediate (I^*). In a classic free diffusion system, the labeled I^* will be diluted by unlabeled I, resulting in a lower specific radioactivity of the labeled product (P^*) relative to that of the labeled substrate (S^*). However, if the intermediate is transferred directly from E_1 to E_2, then the ratio of specific radioactivity of P^* to S^* will be near unity.

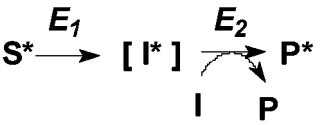

A third protein (E_3) can also be added to the reaction mixture to probe for the dissociation of the intermediate I into the bulk solvent. A large excess of E_3 is included to compete with the activity of E_2 for the reaction intermediate I (Scheme 3). An implicit assumption of this approach is that E_3 remains in the bulk solvent and does not associate with the E_1E_2 complex. Recently, a variation of this approach has been proposed by Geck & Kirsch (18). The reaction is carried out in the presence of a large excess of an inactive variant of E_1. If a direct transfer mechanism is operative, then the inactive E_1 mutant will compete with the wild-type E_1 for the docking sites on E_2 and thus inhibit the tunneling of the reaction intermediate from E_1 to E_2.

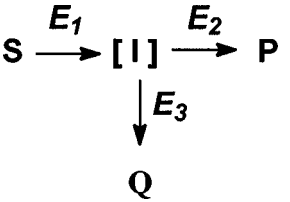

Transient-state kinetic analyses with high enzyme concentrations can, in principle, detect reaction intermediates, products, and other distinct enzyme forms and measure their rates of transformation during the overall reaction. This approach can thus provide higher levels of molecular insight into enzymatic reaction mechanisms than steady-state techniques. There are, however, limitations to this approach. Detectable spectral changes during transitions of enzyme forms are required, as is the availability of suitable forms of reaction intermediates that can be monitored directly. More detailed descriptions of steady-state and transient-state methods as tests for substrate channeling are available in two recent reviews 3, 4).

Many fundamental questions remain unanswered about the mechanisms for substrate channeling. How did the molecular tunnels evolve? Is convergent evolution required for the interaction of protein domains or subunits? If the molecular tunnels evolved gradually, then a perfect channeling system may, in fact, have imperfect or

leaky ancestors. Most multifunctional enzymes and multienzyme complexes are regulated by allosteric communication between the active sites. Does the tunneling event also synchronize the enzymatic reactions occurring at the distinct active sites? What is the mechanism of diffusion through a protein tunnel? Is active transport employed? It is not clear in most cases whether the molecular tunnel adopts different conformational states before and/or during the tunneling event. What governs the directionality for the migration of the intermediate inside the tunnel and what prevents the escape of the intermediates from the tunnel? How fast is the tunneling event?

There is, to our knowledge, no theoretical or experimental calculation for the one-dimensional diffusion of a reaction intermediate through a molecular tunnel. In theory, a one-dimensional diffusion event should require less time than a three-dimensional diffusion process in solution, owing to the reduction in the space that must be sampled. An example analogous to one-dimensional diffusion through a protein tunnel is the linear migration of proteins on DNA. A review of the theoretical aspects of protein diffusion on DNA is available (19). Jeltsch & Pingoud have determined the rate constant for the linear diffusion (k_{diff}) of *Eco*RV restriction endonuclease on DNA (20). A k_{diff} of 1.7×10^6 base pairs (bp) per second was obtained, in apparent agreement with another recent estimate of $>5 \times 10^5$ bp/s (21). The value of k_{diff} is related to the linear diffusion coefficient (D) according to Equation 1 (Fick's law) where l is the length of each step (0.34 nm in B-form DNA). A diffusion coefficient (D) of 9.6×10^{-14} m^2 s^{-1} was obtained using a k_{diff} of 1.7×10^6 bp/s.

$$D = 0.5 k_{diff} l^2 \qquad 1.$$

This is close to the theoretic limit of 5×10^{-13} m^2 s^{-1}, governed by hydrodynamics (22). A rough estimate for the mean diffusion time (τ) for one-dimensional diffusion of 50 Å through a molecular tunnel can be calculated from Equation 2 where L is the distance traveled and D is the diffusion coefficient (23). Assuming that the diffusion coefficient for protein movement on DNA is a good estimate for the tunneling event, then a value for τ of 8.7×10^{-5} s^{-1} is obtained. Therefore, a rate constant of about 11,000 s^{-1} for a migration of 50 Å is obtained. Transient kinetic studies of tryptophan synthase and thymidylate synthase–dihydrofolate reductase have yielded a lower limit of 1000 s^{-1} for tunneling events in these systems (24, 25). It thus appears that tunneling of reaction intermediates is not rate-limiting for overall catalysis.

$$\tau = L^2/3D \qquad 2.$$

EXAMPLES OF SUBSTRATE CHANNELING

Tryptophan Synthase

Tryptophan synthase catalyzes the final two reactions of the biosynthesis of L-tryptophan (for reviews see 26–30). In bacteria, tryptophan synthase exists as

an $(\alpha\beta)_2$ complex. Each α-subunit catalyzes the cleavage of indole 3-glycerol phosphate (IGP) to produce indole and D-glyceraldehyde 3-phosphate, and each β-subunit contains a pyridoxal phosphate moiety that is involved in the formation of L-tryptophan from L-serine and the endogenously generated indole intermediate. To date, all the biochemical data suggest that during the synthesis of L-tryptophan from IGP and L-serine, indole is not released into solution, which is fully consistent with the tunneling of this intermediate from the active site of the α-subunit to that of the β-subunit. Interestingly, the enzyme can also use external indole for the synthesis of L-tryptophan. Tryptophan synthases from higher plants also exist as $(\alpha\beta)_2$ complexes, whereas the enzymes from yeast and molds are single bifunctional proteins with the homologous α and β regions covalently connected by linker peptides (31–33).

Direct physical evidence for the tunneling of indole in tryptophan synthase was first provided by the elegant X-ray structural analyses of the enzyme from *Salmonella typhimurium* (34, 35). As can be seen in Figure 1, the quaternary structure of the $(\alpha\beta)_2$ complex is nearly linear; the two β-subunits are tightly associated in the center of the molecule and the two α-subunits are situated on opposite sides of the $\beta\beta$ dimer (34). This three-dimensional arrangement of the four subunits leads to an overall length of $\sim$50 Å. The α-subunit, containing 268 amino acid residues, folds into a single domain that contains 8 parallel β-strands and 13 α-helices in a classical TIM (named for triosephosphate isomerase) barrel topology. As observed in other TIM-barrel enzymes, the active site of the α-subunit is located at the C-terminal portion of the β-sheet where the competitive inhibitor, indole propanol phosphate, was observed to bind in the original structural analysis of the enzyme (34). In contrast to the α-subunit, the

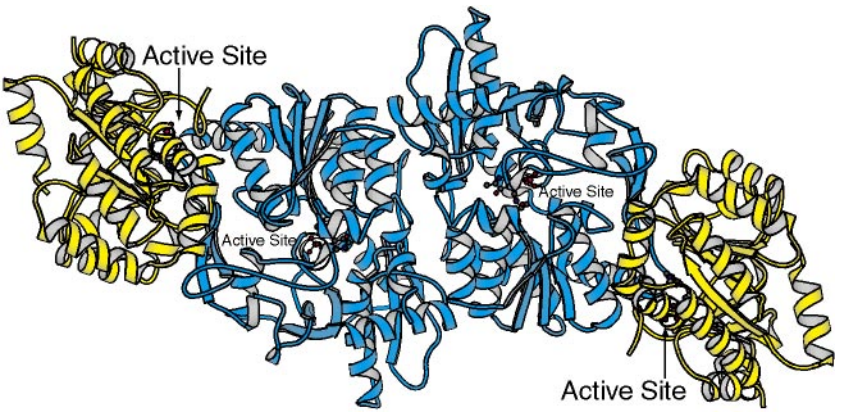

Figure 1 Ribbon representation of the $(\alpha\beta)_2$ complex of tryptophan synthase. The α- and β-subunits are color-coded in yellow and cyan, respectively. The two-fold rotational axis relating the heterodimers is perpendicular to the plane of the page. X-ray coordinates employed for this representation were obtained from the Protein Data Bank (2TRS).

β-subunit is distinctly bilobal, with the N- and C-terminal domains of nearly equal size (34). The N-terminal motif is dominated by a four-stranded parallel β-sheet, and the C-terminal domain is characterized by a six-stranded mixed β-sheet. Pyridoxal phosphate is positioned at the interface between these two structural domains. Quite strikingly, the two active sites in the α/β pairs of the tryptophan synthase $(\alpha\beta)_2$ complex are separated by $\sim$5 Å and are connected by a largely hydrophobic tunnel, as shown in Figure 2. This tunnel extends from the active site of the α-subunit to the center of the molecular interface between the N- and C-terminal domains of the β-subunit and then proceeds to the center of the binding site for pyridoxal phosphate (34). Most of the tunnel is contained within the β-subunit and, interestingly, the tunnel can accommodate up to four indole molecules. The tunnel appears to have molecular dimensions compatible with its putative role as

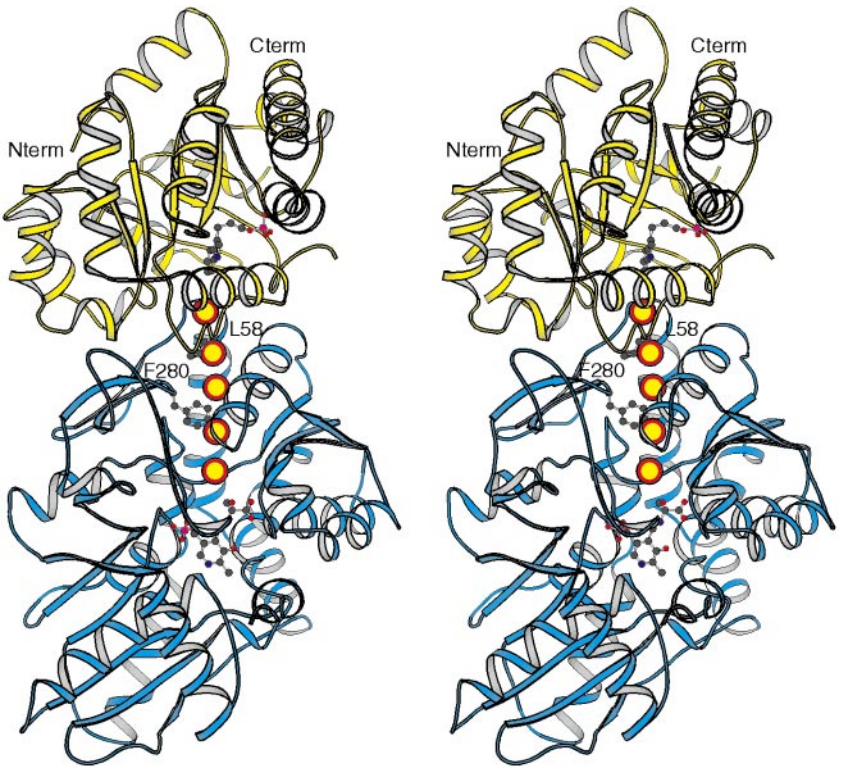

Figure 2 Stereoview of one $(\alpha\beta)$-heterodimer of tryptophan synthase. As in Figure 1, the α- and β-subunits are yellow and cyan, respectively. The α-subunit contains bound indole-3-propanol phosphate and the β-subunit contains L-serine, which forms an aldimine with the coenzyme pyridoxal phosphate. The orange spheres represent the course of the tunnel running from the α- to the β-subunits. This tunnel is $\sim$25 Å long.

a conduit for indole. Subsequent higher-resolution structural analyses revealed two sites along the tunnel that are partially blocked. At one site, Phe-280 in the β-subunit inserts directly into the channel (35). Strikingly, exchange of potassium or cesium ions for sodium ions results in a movement of this Phe-280 side chain out of the tunnel, which suggests that this residue may indeed play a role as a molecular gate (35). The second site of close interaction along the tunnel occurs at Leu-58 in the α-subunit. In the native structure, however, this region of the polypeptide chain is fairly mobile, as suggested by the higher-than-average temperature factors. Clearly, molecular dynamics play a role in the proper functioning of the tunnel in tryptophan synthase. As can be seen in Figure 2, the two active sites are arranged in a manner that suggests that both IGP and D-glyceraldehyde 3-phosphate enter and exit through a "front door" in the α-subunit, and L-serine and L-tryptophan enter and exit via a front door in the β-subunit. The back doors of the two active sites lead to the tunnel, which allows for the diffusion of the intermediate, indole (35).

In the original investigation of tryptophan synthase, the electron density corresponding to a surface loop in the α-subunit, namely that delineated by Leu-177 to Ala-190, was disordered. Subsequent X-ray crystallographic studies of a site-directed mutant protein (βK87T) with various combinations of ligands bound in the two active sites revealed several important conformational changes that are most likely important for the regulation of the enzyme activity (36). Specifically, when either α-glycerol 3-phosphate or indole-3-propanol phosphate are bound to the α-subunit (and the β-subunit active site is also occupied), the disordered surface loop becomes ordered and clamps down over the active site, thereby isolating this region from solvent. Other conformational changes that occur upon ligand binding include a rigid body rotation of the α-subunit relative to the β-subunit by $\sim 5^{\circ}$ and large movements of part of the β-subunit (Gly-93 to Gly-189). These changes have been suggested to restrict the access of solvent to the active sites in the ($\alpha\beta$)-pair and to the tunnel and, as such, may also be critically important for preventing indole from escaping into the surrounding milieu (37).

Reaction Mechanism of Tryptophan Synthase Tryptophan synthase is a member of the pyridoxal phosphate–requiring enzymes. The condensation of L-serine and indole at the active site of the β-subunit is a classical pyridoxal phosphate–dependent β-replacement reaction (38). The reaction mechanism has been well characterized by both steady-state and transient-state kinetic approaches (24, 39–41), and most of the intermediates have been identified by their spectral properties. In the absence of L-serine, the cofactor pyridoxal phosphate is covalently bound to the ε-amino group of Lys-87 of the β-subunit. Transimination between L-serine and pyridoxal phosphate results in the formation of an external aldimine intermediate, and then deprotonation leads to a quininoid intermediate. This step is followed by the elimination of a water molecule to form an aminoacrylate intermediate. Condensation of the aminoacrylate intermediate with internal (or external) indole generates a second quininoid intermediate that is protonated to produce a second

external aldimine intermediate. Subsequent release of the product, L-tryptophan, completes the catalytic cycle (42).

Kinetic Evidence for Tunneling of Indole Evidence for the tunneling of indole in tryptophan synthase comes from steady-state experiments that failed to trap indole as an intermediate in the overall reaction (43–46). Recently, kinetic evidence has been provided by the elegant work of Anderson, Dunn, Miles, and coworkers using transient-state kinetic approaches including chemical quench-flow and stopped-flow methods (24, 47). In a single-turnover experiment monitoring the overall conversion of IGP and L-serine to L-tryptophan, only a trace of indole ($\leq$1% of IGP) was detected, and a lag in the formation of L-tryptophan was absent (24). This result is consistent with the tunneling of the indole intermediate. Diffusion of indole into the bulk solution would have resulted in a buildup of indole and a subsequent lag in the formation of L-tryptophan. Detailed kinetic analyses indicate that indole moves quickly from the active site of the α-subunit to that of the β-subunit ($\geq$1000 s^{-1}) and reacts rapidly ($\geq$1000 s^{-1}) with the aminoacrylate intermediate to form L-tryptophan at the β-site (24).

Two important features of the tunneling event were tested by site-directed mutagenesis. If the rate of migration of indole through the molecular tunnel could be slowed or if the rate of reaction with the aminoacrylate intermediate could be diminished, then the tunneling of indole would be made more inefficient. Consequently, indole would build up as a detectable intermediate and the formation of L-tryptophan would display a lag. Glu-109 in the β-subunit has been proposed to play a critical role in the activation of indole toward nucleophilic attack on the aminoacrylate intermediate (24, 35). In the βE109D mutant protein, the condensation of indole and the aminoacrylate intermediate is slowed by 300-fold in comparison to the wild-type enzyme (24). According to the X-ray structure of tryptophan synthase, Cys-170 of the β-subunit contributes to the formation of the intact tunnel wall. Changing Cys-170 to either a phenylalanine or tryptophan residue was expected to impede the free passage of indole through the molecular tunnel. Kinetic data are consistent with a reduction in the rate of channeling for these two mutants (48, 49). The βC170W mutant protein is impaired in intersubunit communication because the cleavage of IGP at the α-site is no longer stimulated in the overall reaction. In single-turnover experiments with the βE109D, βC170F, or βC170W mutant proteins, indole buildup and a lag in L-tryptophan formation were observed (24, 49). Clearly, the rapid migration and reactivity of indole at the β-subunit with the aminoacrylate intermediate are essential for the efficient coupling of the two active sites within tryptophan synthase.

Allosteric Communication Between the α- and β-Sites Efficient substrate channeling in tryptophan synthase requires not only the physical presence of a tunnel, a rapid tunneling event, and a rapid β-reaction but also the synchronization of the catalytic activities at both the α- and β-subunit active sites. In the absence of L-serine, the cleavage of IGP at the active site of the α-subunit of tryptophan

synthase is very slow. Numerous experiments have indicated that ligand binding to the active site of the β-subunit alters the kinetics of the α-reaction. Steady-state analyses have found that the reaction of L-serine at the β-site decreases the K_m for IGP and stimulates the cleavage of IGP by 20- to 30-fold at the α-site (43). Transient kinetic studies by Anderson et al have firmly established that the reaction of L-serine at the β-site modulates the formation of indole at the active site of the α-subunit (24). The formation of the aminoacrylate intermediate triggers the activation of the α-reaction (24). A lag in the cleavage of IGP was predicted and observed in a single-turnover experiment in which L-serine and IGP were added simultaneously to tryptophan synthase. The kinetics of the lag match that of the formation of the aminoacrylate intermediate. There was also a change in protein fluorescence, coincident with the formation of the aminoacrylate intermediate, although such fluorescence measurements may be complicated by the fluorescence of the reaction intermediates and possible fluorescence energy transfer. Taken together, these data suggest that the formation of the aminoacrylate intermediate at the β-subunit active site results in a protein conformational change that is transmitted to the α-subunit site, where it triggers the enhancement of IGP cleavage. Recent results of Leja, Woehl & Dunn indicate that the conversion of the quininoid intermediate to the external aldimine intermediate is the chemical signal that deactivates the active site of the α-subunit (47). Kirchner et al took advantage of 6-nitroindole glycerol 3-phosphate, an IGP analog, whose cleavage product, 6-nitroindole, does not react with L-serine (50). These two allosteric features of tryptophan synthase ensure that indole is produced only when the β-site is ready to receive it. It thus appears that this allosteric modulation of the catalytic activity of the α-subunit by chemical events occurring at the β-subunit active site is also an essential element required for efficient tunneling of indole between the two polypeptide chains.

The allosteric communication between the α- and β-subunits appears to be reciprocal. The binding of an α-ligand (indole 3-propanol phosphate or α-glycerol 3-phosphate) to the α-subunit increases the affinity of the β-subunit active site for amino acids and alters the steady-state distribution of reaction intermediates at the β-site (51, 52). A recent luminescence study demonstrates that α-glycerol 3-phosphate bound at the α-site leads to a more rigid structure in the β-subunit (53). Whether the molecular changes occurring at the α-site contribute to the efficient tunneling of indole and the coupling of two catalytic activities in tryptophan synthase is presently unclear.

Dunn and coworkers demonstrated that the reaction between external indole and L-serine was strongly inhibited by α-glycerol 3-phosphate, an IGP analog (39, 40, 47). These results are consistent with the hypothesis that external indole also enters through the α-subunit and the intramolecular tunnel. These inhibitory efforts were reversed by mutations in either loop-2 or loop-6 of the α-subunit (40, 54). Most likely, the normal function of these loops is to close off the active site of the α-subunit, which prevents the escape of indole into the bulk solution (40, 54). Studies of the conformational states of tryptophan synthase during

catalysis employing 8-anilino-1-naphthalene sulfonate (ANS) suggest that chemical signals from the β-site serve not only to synchronize the two distinct catalytic events but also to trigger the shuffling between open and closed enzyme forms (55).

In summary, efficient substrate channeling in tryptophan synthase is a result of the following four essential elements: (*a*) the physical presence of a hydrophobic tunnel connecting the active sites of the α- and β-subunits; (*b*) the rapid rate of the channeling event; (*c*) the rapid rate of the condensation reaction at the β-site; and (*d*) the allosteric communication between the two sites that results in full coupling of the reaction at the α- and β-subunits.

Carbamoyl Phosphate Synthetase

Carbamoyl phosphate serves as a precursor for two important metabolic pathways: the biosynthesis of arginine and urea, and the de novo production of pyrimidine nucleotides. In the urea cycle and in arginine biosynthesis, the carbamoyl moiety of carbamoyl phosphate is transferred to ornithine, whereas in the pyrimidine pathway the same group is condensed with aspartate. Three different types of carbamoyl phosphate synthetases (CPSs) have been identified thus far, based on their preference for glutamine or ammonia as their nitrogen source and the requirement for *N*-acetyl-L-glutamate (NAcGlu) for activity (56). Type I CPS requires free ammonia as the nitrogen source and is involved in arginine biosynthesis and the urea cycle. Additionally, the enzyme requires NAcGlu for activity. Types II and III CPS prefer glutamine as the physiological nitrogen source. Type III CPS requires the presence of NAcGlu for activity, but Type II does not. In prokaryotes such as *Escherichia coli*, there is only one CPS, usually a Type II protein, for both biosynthetic pathways. In higher eukaryotes, a Type I or III enzyme is involved in the urea cycle and in arginine biosynthesis and a Type II enzyme participates in pyrimidine production. The Type II enzyme exists as part of a multifunctional protein referred to as CAD that contains, in addition to CPS activity, aspartate transcarbamoylase and dihydroorotase functionalities (57). (Reviews of carbamoyl phosphate synthesis can be found in 56, 59.)

Carbamoyl phosphate synthetase from *E. coli* is a heterodimeric protein composed of a small amidotransferase subunit (with a molecular mass of $\sim$42 kilodaltons) and a large synthetase subunit ($\sim$118 kilodaltons). The enzyme readily converts to an $(\alpha\beta)_4$-tetrameric species depending on the presence or absence of various effectors. CPS assembles carbamoyl phosphate from bicarbonate, glutamine, and two molecules of ATP as shown in Equation 3. The enzyme is a member of the Triad class of glutamine amidotransferases, which also includes anthranilate synthase, GMP synthetase, and CTP synthetase, among others (60, 61). The binding sites for glutamine within this family of amidotransferases contain a strictly conserved Cys-His couple. These enzymes initiate the hydrolysis of glutamine at one active site and then transfer the ammonia product to an acceptor site within the same protein (61). The overall synthesis of carbamoyl phosphate has

been proposed to occur within the three active sites of CPS via four distinct chemical steps and three reactive intermediates as illustrated in Scheme 4, discussed in the next subsection (62). The small subunit of CPS hydrolyzes glutamine to glutamate and ammonia through the intermediacy of a thioester with the catalytic Cys-269 (63–65). The large subunit of CPS assembles carbamoyl phosphate via consecutive events of phosphorylation of bicarbonate and carbamate. In addition to the overall reaction, CPS also catalyzes three partial reactions when one or more of the substrates are absent from the reaction mixture. These partial reactions are summarized in Equations 4–6 (62). Ammonia can substitute for glutamine in the overall reaction as an alternative source of nitrogen (Equation 7).

$$2\,\mathrm{MgATP} + \mathrm{HCO_3^-} + \mathrm{Gln} + \mathrm{H_2O} \rightarrow 2\,\mathrm{MgADP} + \mathrm{P_i} + \mathrm{Glu} + \text{carbamoyl-P} \quad 3.$$

$$\mathrm{Gln} + \mathrm{H_2O} \rightarrow \mathrm{Glu} + \mathrm{NH_3} \quad 4.$$

$$\mathrm{MgATP} + \mathrm{H_2O} \rightarrow \mathrm{MgADP} + \mathrm{P_i} \quad 5.$$

$$\mathrm{MgADP} + \text{carbamoyl-P} \rightarrow \mathrm{MgATP} + \mathrm{NH_2CO_2^-} \quad 6.$$

$$2\,\mathrm{MgATP} + \mathrm{HCO_3^-} + \mathrm{NH_3} + \mathrm{H_2O} \rightarrow 2\,\mathrm{MgADP} + \mathrm{P_i} + \text{carbamoyl-P} \quad 7.$$

The three-dimensional structure of CPS from *E. coli* was solved in 1997 (66); a ribbon representation of the $(\alpha\beta)_4$-heterotetramer is displayed in Figure 3. As color-coded in yellow in Figure 3, the small subunits of the heterotetramer are perched at either end of the molecule. Each small subunit is distinctly bilobal in appearance, with the N-terminal domain formed by Leu-1 to Leu-153 and the C-terminal domain delineated by Asn-154 to Lys-382. Whereas the N-terminal domain is composed primarily of four major α-helices and two layers of β-sheet, the C-terminal motif contains 10 strands of mixed β-sheet with a topology remarkably similar to that of the N-terminal domain of GMP synthetase (66a). The side chain residues, namely Cys-269 and His-353, that are required for the hydrolysis of glutamine to glutamate and ammonia are positioned within the interface of these two domains. With regard to the large subunit, the three-dimensional structural analysis confirmed that it contains distinct active sites for the phosphorylation of bicarbonate and carbamate (66, 67). The carboxy phosphate (Met-1 to Glu-403) and carbamoyl phosphate (Asn-554 to Asn-936) domains of the large subunit share ~40% amino acid sequence identity (68), and structurally belong to the so-called ATP-grasp superfamily (66). Both the carboxy phosphate and carbamoyl phosphate domains can be further broken down into smaller motifs referred to as the A-, B-, and C-subdomains.

By far the most remarkable feature of the molecular architecture of CPS is the location of the three active sites contained within the heterodimer (66). Indeed, the active site in the small subunit is located at ~45 Å from the active site in the carboxy phosphate domain of the large subunit, which in turn is situated ~35 Å from the active site in the carbamoyl phosphate motif. Visual inspection of the CPS model and a computational search with the software package GRASP has identified

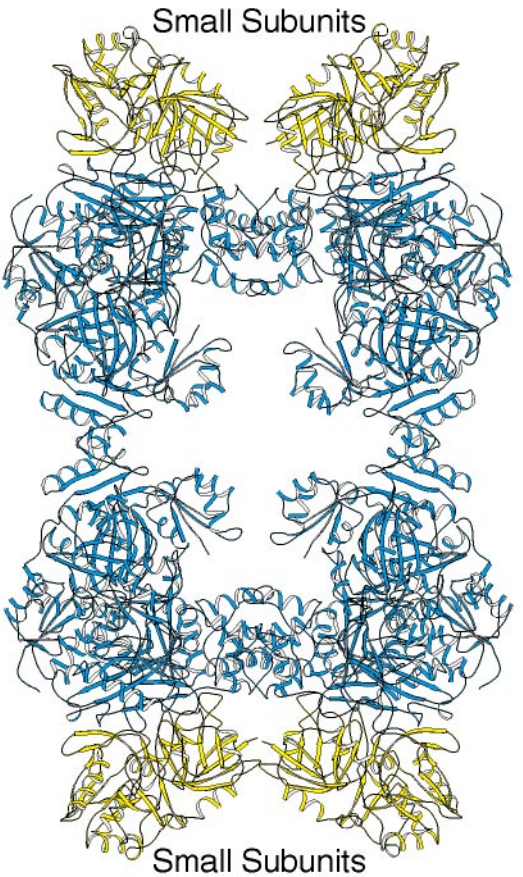

Figure 3 Ribbon representation of the CPS $(\alpha\beta)_4$-tetrameric species. The CPS $(\alpha\beta)_4$-tetrameric species displays 222 symmetry with one of the molecular dyads oriented perpendicular to the plane of the page and the other two lying within the plane. The small subunits are displayed in yellow and the large subunits are in cyan. As expected for an assembly that readily interconverts between an $(\alpha\beta)$-heterodimer and an $(\alpha\beta)_4$-tetrameric species, the interfacial regions between the four $\alpha\beta$-motifs are quite small. X-ray coordinates used for this figure were obtained from the Protein Data Bank (1JDB).

a molecular tunnel within the interior of the heterodimeric protein, which leads from the base of the glutamine binding site within the small subunit toward the two phosphorylation sites of the large subunit, as indicated in Figure 4 (66, 67). Accordingly, the ammonia produced at the active site of the small subunit traverses the first half of this molecular tunnel to react with the carboxy phosphate intermediate formed at the first ATP binding site of the large subunit. With the exception of Glu-217 and Cys-232, the tunnel leading from these first two active

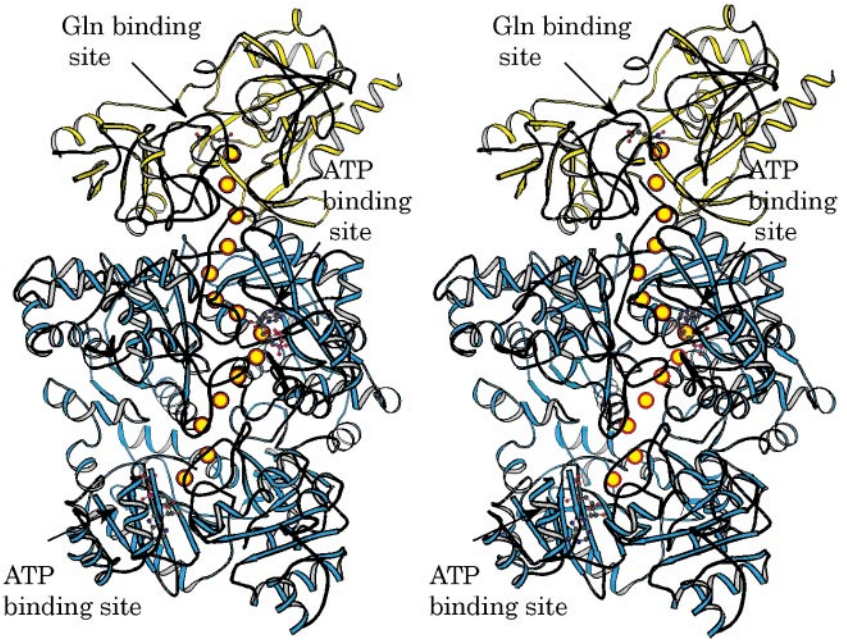

Figure 4 Stereoview of the $(\alpha\beta)$-heterodimer of CPS. The yellow spheres trace the course of the molecular tunnel that leads from the active site of the small subunit to the first ATP binding site of the large subunit, and finally to the second ATP binding pocket. A linear distance of ~80 Å separates the active site of the small subunit from the second ATP binding region of the large subunit.

sites of the heterodimer is lined primarily with unreactive side chains and backbone atoms. Once formed, the carbamate intermediate diffuses through the next part of the molecular tunnel to react with the second molecule of ATP. This part of the molecular tunnel is somewhat less hydrophobic and includes side chains contributed by Glu-577, Glu-604, Arg-848, Lys-891, and Glu-916 (67). There are approximately 25 water molecules lying within 2 Å of the pathway, but their actual positions during catalysis are unknown. Strikingly, many of the residues lining the tunnel are absolutely conserved among 22 of 24 primary structural alignments of CPS (69), and many of the residues that are not strictly conserved are replaced with amino acid residues of comparable chemical reactivities. Recent reviews of CPS structure and function are available (69–71).

Intermediacy of the Three Reactive Species The chemical mechanism shown in Scheme 4 proposes the existence of three reactive intermediates during the course of carbamoyl phosphate synthesis: carboxy phosphate, ammonia, and carbamate. The occurrence of carboxy phosphate is supported by the observation of

a bicarbonate-dependent ATPase reaction (Equation 5). This reaction is approximately one order of magnitude slower than the overall synthetic reaction with glutamine as the nitrogen source. When the bicarbonate is labeled with ^{18}O, one of three labeled oxygen atoms is transferred to the phosphate product (72). This result is consistent with an attack of the carboxy phosphate intermediate on the carbonyl carbon by water. The kinetic competency of the carboxy phosphate intermediate has been confirmed by positional isotope exchange and rapid-quench experiments (72–75).

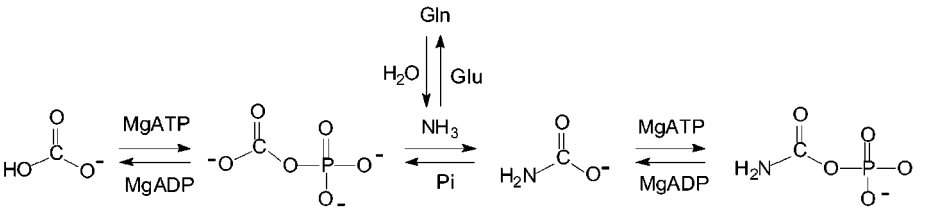

The occurrence of ammonia as a reaction intermediate is supported by the observation of the hydrolysis of glutamine to glutamate and ammonia in the absence of MgATP or bicarbonate (Equation 4). This reaction is approximately two to three orders of magnitude slower than the overall synthesis of carbamoyl phosphate in the presence of MgATP and bicarbonate (63). Recent rapid-quench experiments have confirmed that the steady-state formation of glutamate is synchronous with that of carbamoyl phosphate during the overall reaction (76). The intermediacy of ammonia is also supported by the observation that ammonia can substitute for glutamine as a direct nitrogen source in the overall synthesis of carbamoyl phosphate with comparable turnover numbers (77).

The formation of carbamate during the course of carbamoyl phosphate synthesis is postulated largely upon the observation of the formation of MgATP from MgADP and carbamoyl phosphate (Equation 6). Measurement of proton release during this partial reaction provides evidence for the formation of carbamate (78). Raushel & Villafranca showed that enzymatic bridge:nonbridge exchange in ^{18}O-labeled carbamoyl phosphate in the presence of MgADP is four times faster than the net synthesis of MgATP (73). This result is consistent with the formation of carbamate.

The pH activity profiles of CPS indicate that enzyme-bound NH_3 must be sequestered from the bulk solvent at physiological pH because NH_4^+ does not react with carboxy phosphate (79, 80). Wang et al have estimated that the half-life of carbamate at neutral pH is 70 ms (81). This renders it highly improbable that carbamate dissociates from the first phosphorylation site, enters the bulk solvent, and then reassociates with the second phosphorylation site of the large subunit of CPS. Based on the reactive nature of both ammonia and carbamate, the relative location of the three active sites in the structure of CPS, and the identification of its long molecular tunnel, it is logical to assume that ammonia

and carbamate are tunneled from their sites of generation to their respective sites of use.

Kinetic Evidence for Tunneling of Ammonia In an isotope competition experiment monitoring the formation of [^{15}N]-carbamoyl phosphate from a mixture of 100 mM $^{15}NH_4Cl$ and 25 mM unlabeled glutamine, Mullins & Raushel showed that the incorporation of ^{15}N in the product is 4.8% (82). If the NH_3 derived from the hydrolysis of glutamine fully equilibrates with the $^{15}NH_3$ in the bulk solvent, then the expected incorporation ratio is at least 80%. These results suggest that the internal ammonia, derived from the hydrolysis of glutamine, is not in equilibrium with the external ammonia in the bulk solvent; rather it is sequestered and channeled directly to the large subunit. The likely explanation for the difference between the observed value (4.8%) and the theoretical value (0.6%) is minor uncoupling of the partial reactions occurring on the small and large subunit of CPS during these experiments (82).

More direct support for the tunneling of ammonia within the interior of CPS has been provided by studies of mutants created to block the molecular tunnel within the enzyme (83). In these studies, residues that define the interior walls of the "ammonia tunnel" within the small subunit of CPS were modified to either block or impede the passage of ammonia to the large subunit. With the G359F and G359Y site-directed mutant proteins, the hydrolysis of glutamine occurring within the small subunit became almost completely uncoupled from the bicarbonate-dependent hydrolysis of ATP occurring within the large subunit. Both of these mutant proteins lost the ability to synthesize carbamoyl phosphate. However, they were fully functional when external ammonia was provided as the nitrogen source, suggesting the existence of an alternate route to the bicarbonate phosphorylation site.

In a recent follow-up study expanding on an earlier approach, a series of proteins was created with site-directed mutations within the ammonia tunnel. The degree of constriction within the ammonia tunnel of these enzymes was found to correlate with the extent of the uncoupling of the partial reactions, the diminution of carbamoyl phosphate formation, and the percentage of the internally derived ammonia that was channeled through the ammonia tunnel (84). Kinetic results indicated that hydroxylamine, derived from the hydrolysis of γ-glutamyl hydroxamate, an analog of glutamine, was also channeled through the ammonia tunnel to the large subunit (84). Discrimination between the passage of ammonia and hydroxylamine was observed among some of these tunnel-impaired enzymes. Overall, these results provide compelling evidence for the tunneling of ammonia within native CPS.

Kinetic Evidence for Tunneling of Carbamate Currently the evidence for the tunneling of carbamate comes largely from the crystal structure of CPS (66, 67). Recent experiments demonstrated that there was no ^{18}O isotope exchange reaction between solvent water and bicarbonate during the overall synthesis of carbamoyl

phosphate with glutamine as the nitrogen source (85). These data suggest that all of the carbon-containing intermediates (carboxy phosphate and carbamate) are fully committed to the formation of carbamoyl phosphate and not subjected to hydrolysis. Experiments have provided preliminary evidence for carbamate channeling through the tunnel-blockage strategy (X Huang & FM Raushel, unpublished data). It was found that the replacement of Ala-23 of the large subunit with a leucine residue did not appreciably perturb the three partial reactions occurring at their respective active sites. Interestingly, however, the passage of the carbamate intermediate was significantly impeded, although the allosteric communication between the small subunit and the large subunit remained intact.

Allosteric Communication Between the Three Catalytic Sites of Carbamoyl Phosphate Synthetase The reaction stoichiometry dictates the precise coupling of the individual parallel and sequential chemical events during the assembly of carbamoyl phosphate. Recent rapid-quench experiments have shed some light on this complex process (76). The results are consistent with a mechanism whereby the formation of carboxy phosphate triggers a conformational change that is transmitted to the small subunit where the hydrolysis of glutamine is stimulated (76). The observed enhanced ATPase rate in the presence of glutamine is not due to an increased rate of the phosphorylation of bicarbonate; rather, it merely reflects the faster rate of attack on the carboxy phosphate by the ammonia intermediate relative to water. Thus, ammonia is not released until carboxy phosphate is ready to form carbamate. This appears to be a common feature between CPS and tryptophan synthase. It is currently not clear if or how the second ATP binding site of the large subunit participates in allosteric communication with the other two active sites of CPS (87–90).

Channeling of Carbamoyl Phosphate in Mammalian CAD Complex In mammalian systems, the Type II CPS is part of the so-called CAD enzyme complex. This is a single polypeptide that also encodes aspartate transcarbamoylase and dihydroorotase, the next two enzymes involved in the pyrimidine pathway (60, 61). Some evidence suggests that the product of CPS, carbamoyl phosphate, which itself is unstable at neutral pH, is not released into the bulk solvent but rather is directly channeled to the aspartate transcarbamoylase domain of CAD to form carbamoyl aspartate.

GMP Synthetase

GMP synthetase, like CPS, is a member of the Triad class of glutamine amidotransferases. As the name implies, GMP synthetase catalyzes the formation of GMP from XMP, glutamine, and one molecule of ATP (Equation 8). The GMP synthetase from *E. coli* is a bifunctional enzyme and consists of a glutaminase domain (Met-1 to Ala-206) that is responsible for the hydrolysis of glutamine, and an ATP pyrophosphatase domain (Leu 207-Pro 406) that is responsible for

ATP hydrolysis and GMP formation. As with CPS, the hydrolysis of glutamine by GMP synthetase proceeds through a thioester intermediate with a catalytic cysteine residue (91).

$$\text{XMP} + \text{ATP} + \text{glutamine} + \text{H}_2\text{O} \rightarrow \text{GMP} + \text{AMP} + \text{glutamate} + \text{PP}_\text{i} \quad 8.$$

The X-ray crystal structure of GMP synthetase from *E. coli* was recently solved and shows that the active sites for the glutaminase and the ATP pyrophosphatase domains are separated by 30 Å and are solvent exposed (66a). A clearly defined pathway for the transfer of the ammonia intermediate from the glutaminase motif to the ATP pyrophosphatase domain is not immediately apparent from this structure. It has been proposed, however, that a major structural change occurs upon the binding of MgATP and XMP that is both necessary to stimulate catalysis at the glutaminase domain and to form a channel connecting the active sites of these two domains (61, 66a). Though belonging to the same subfamily of glutamine amidotransferases, GMP synthetase apparently employs a different approach from that of CPS to deliver ammonia from one catalytic site to another.

In addition to CPS and GMP synthetase, other members of the Triad class of amidotransferases include CTP synthetase, anthranilate synthase, PABA synthase, *p*-aminobenzoic acid formylglycinamide ribonucleotide synthetase, imidazole glycerol phosphate synthase, NAD synthetase, and aminodeoxychorismate synthase (60, 61). The specific strategies used in these amidotransferases to couple the glutaminase and the synthetase activities together is presently unknown. Thus far a total of ten residues in the small subunit of CPS have been identified that appear to constitute the interior walls of the ammonia tunnel (83). Of these ten residues, three are located within the N-terminal domain of the small subunit, which is structurally unique in comparison with other members of the Triad amidotransferases. The other seven residues, located within the C-terminal amidotransferase domain of the small subunit, are either strictly conserved or replaced with residues of comparable size and reactivity among all known carbamoyl phosphate synthetases. However, none of the seven residues is conserved among the other Triad amidotransferases. Clearly, if the channeling of ammonia occurs in these other Triad amidotransferases, the molecular architecture employed for the delivery of ammonia will be quite different from that observed in CPS.

Glutamine Phosphoribosylpyrophosphate Amidotransferase

Glutamine phosphoribosylpyrophosphate amidotransferase (GPATase) catalyzes the first committed step in the de novo synthesis of purine nucleotides. The enzyme converts glutamine and phosphoribosylpyrophosphate (PRPP) to phosphoribosylamine (PRA), glutamate, and pyrophosphate (Equation 9).

$$\text{Glutamine} + \text{PRPP} \rightarrow \text{PRA} + \text{glutamate} + \text{PP}_\text{i} \quad 9.$$

Like CPS, GPATase is a glutamine amidotransferase, albeit a member of a different class, the so-called N-terminal nucleophile (Ntn) family. This particular class of enzymes employs an essential N-terminal cysteine residue that serves as both the nucleophile that attacks glutamine and the general base that protonates the amide leaving group (60, 61, 93). Similar to the observed allosteric regulation of CPS by ornithine and UMP, GPATase is subjected to feedback inhibition by the end products of purine synthesis such as AMP and ADP. GPATases from *E. coli* and *Bacillus subtilis* have been purified to homogeneity and characterized (94, 95). Based on the alignment of all known GPATase sequences, two classes emerge for these enzymes, represented respectively by the *B. subtilis* enzyme, which has an N-terminal propeptide and an [Fe-S] cluster, and the *E. coli* enzyme, which lacks both of these features (61). The cleavage of the propeptide is required for the generation of the active form of the *B. subtilis* enzyme. The [Fe-S] cluster in the *B. subtilis* enzyme has been proposed to regulate the turnover rate of this protein in vivo (96–98). Because the X-ray crystal structures of the AMP-bound GPATases from *E. coli* and *B. subtilis* are very similar (99, 100), it is generally assumed that these two classes of GPATases employ similar catalytic mechanisms. In the *E. coli* enzyme, both dimeric and tetrameric species have been observed in solution. A ribbon representation of the dimeric species is displayed in Figure 5. Each subunit of the *E. coli* enzyme is divided into two motifs: the N-terminal domain delineated by Cys-1 to Ile-230 and the C-terminal region defined by Tyr-231 to Tyr-465. The N-terminal domain contains two antiparallel β-sheets flanked on the outer edges by α-helices, and the C-terminal motif is dominated by a five-stranded parallel β-sheet.

Unlike CPS, but similar to GMP synthetase, the two catalytic domains of GPATases from *E. coli* and *B. subtilis* are encoded as single polypeptides. In the overall reaction, the N-terminal glutaminase domain of GPATase catalyzes the hydrolysis of glutamine and delivers the ammonia intermediate to the C-terminal synthetase domain of the same protein (93, 101, 102), where the nucleophilic attack of PRPP by ammonia yields PRA and pyrophosphate (103). In the absence of PRPP, the basal rate of glutamine hydrolysis is very slow. The binding of PRPP stimulates the glutaminase activity, mostly through lowering the K_m for glutamine by over 100-fold (102). This allosteric feature ensures that the catalytic reactions at the two distal sites are fully coupled to one another. As with other amidotransferases, NH_3, rather than NH_4^+, is the substrate for the second half-reaction of GPATase (94).

Structural Evidence for Tunneling of Ammonia The three-dimensional structures of GPATase from *E. coli* without bound ligands, with bound AMP, or with bound 6-diazo-5-oxonorleucine (DON), a glutamine affinity analog, are essentially identical (100, 102). These structures are very similar to that of GPATase from *B. subtilis* with bound AMP (99). All four of these structures likely represent inactive forms of GPATase, as they appear incompatible with efficient catalysis. In all of the X-ray models, the PRPP sites are exposed to the bulk solvent. Additionally, the signature flexible loop (Lys-326 to Leu-350) of the synthetase

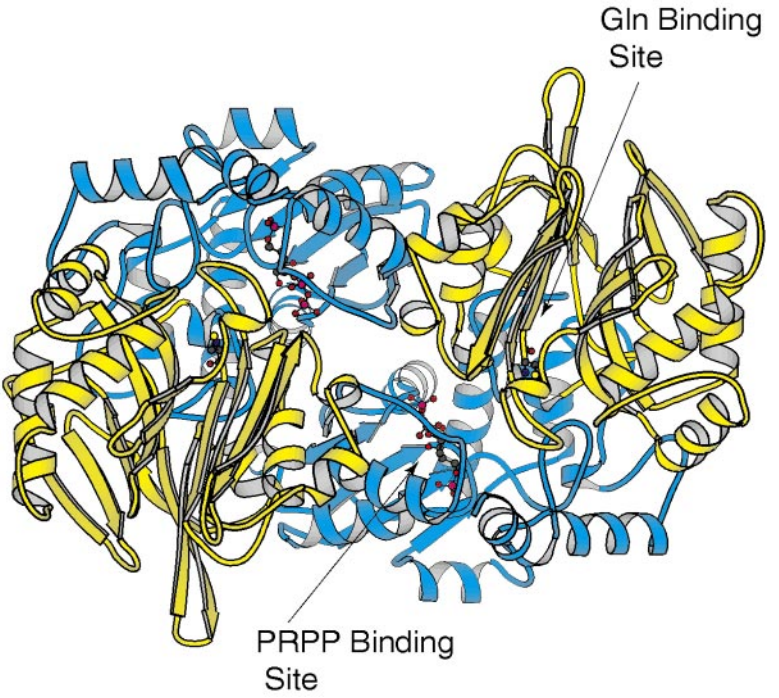

Figure 5 Ribbon representation of the GPATase dimer. X-ray coordinates used for this figure were obtained from the Protein Data Bank (1ECC). Each subunit of GPATase consists of an N- and a C-terminal domain. The N-terminal motif (yellow) contains the glutaminase activity and the C-terminal region (cyan) contains the synthetase portion of the molecule. The two-fold rotational axis relating one subunit to another in the dimer is perpendicular to the plane of the page.

domain, thought to sequester the PRPP site from bulk solvent in other phosphoribosyltransferases (PRTase), adopts a flag conformation in the *B. subtilis* enzyme and exhibits disordered conformations in the *E. coli* protein. In all cases this loop protrudes into the bulk solvent without significant contacts with other parts of the protein. Additionally, in all of these structures, the glutamine binding site is in a completely closed cavity that appears inaccessible in the three X-ray structures solved in the absence of bound DON. Of particular note, Arg-73, a part of the glutamine specificity pocket, is clearly mispositioned in the structure with bound DON. Finally, the active sites of the glutaminase and the synthetase domains of GPATase are separated in solvent-exposed three-dimensional space by $\sim$16 Å. A significant conformational change is clearly needed to transform this inactive enzyme form into an active species.

Recently Smith and coworkers solved the crystal structure of GPATase from *E. coli* with DON and cPRPP bound at their respective active sites as indicated

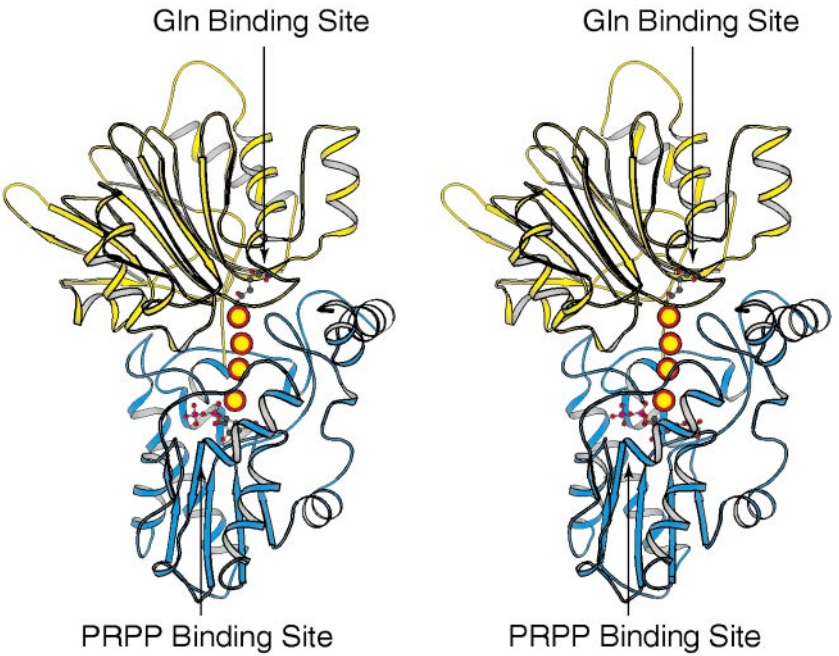

Figure 6 Stereoview of one monomer of GPATase. The yellow spheres represent the molecular tunnel, which is ∼20 Å long and connects the glutamine binding region with the PRPP binding pocket.

in Figure 6 (104). cPRPP is a stable carbocyclic analog of the unstable substrate PRPP (105). The binding of a PRPP analog to the synthetase site leads to the formation of a molecular tunnel of ∼20 Å, which links the two active sites in GPATase. The course of this ammonia conduit is indicated by the orange spheres in Figure 6. The formation of this tunnel results from a kinking of the C-terminal helix, a restructuring of the glutamine loop (Arg-73 to Ser-79), and an ordering of the flexible surface loop formed by Val-325 to Arg-354. Additionally, Arg-73 is repositioned to form a salt bridge with the carboxylate of DON. The 20-Å-long tunnel, which appears large enough in diameter to transport ammonia from the glutamine domain to the PRPP domain, is packed largely by hydrophobic side chains. This contrasts sharply with the relatively hydrophilic ammonia tunnel in CPS (66, 67). The tunnel in CPS appears to be a permanent structural feature, whereas the tunnel observed in GPATase exists only transiently during each catalytic cycle. Strikingly, 14 of the 17 amino acid residues along the pathway in GPATase are invariant in the 24 reported amino acid sequences (104). Clearly, although different glutamine amidotransferases employ distinct strategies for the delivery of the ammonia intermediate, the particular strategy developed within one enzyme seems to be preserved across species.

Tryptophan Fluorescence Studies Uncover an Intermediate Conformational State of GPATase The structure of GPATase with bound substrate analogs, although informative, does not reveal two important molecular features. First, how does glutamine gain access to the glutamine binding site since it is apparently closed off in both the inactive and active states? Second, how does PRPP binding trigger the activation of glutamine hydrolysis and the formation of the transient tunnel? Attempts to address these issues were made by monitoring the steady state and pre-steady-state changes in tryptophan fluorescence of an engineered GPATase with a single tryptophan residue (106, 107). For these investigations, the single tryptophan residue (Trp-290) in the wild-type enzyme was mutated to a phenylalanine and the catalytic Cys-1 was changed to a serine. A tryptophan reporter was then introduced into each of three structural elements that accompany the activation of the enzyme, namely the flexible loop (S345W), the glutamine loop (A82W or S83W), and the C-terminal helix (F477W or R482W). The effects of these modifications on catalytic activities were relatively modest. An increase in the fluorescence intensity of the S345W GPATase, upon the binding of PRPP, was observed (107). Such an increase is often caused by the diminished solvent accessibility to the fluorophore, which is likely due to the ordering of the flexible loop, as observed in the structure of the active form of GPATase. This result is thus consistent with the formation of an intermediate conformational state identified as the enzyme-PRPP complex, which is ready to accept the second substrate, glutamine. A further increase in fluorescence upon the binding of glutamine was observed, which indicates additional repositioning of the flexible loop. Although both Trp-82 and Trp-477 failed to sense the binding of PRPP, each was able to detect the formation of the ternary complex (107). Trp-82 and Trp-482 detected the binding of PRPP and the additional binding of glutamine, as evidenced by the observed fluorescence quenching (106). Collectively, these results are consistent with the proposed tunnel identified in the various X-ray structures of GPATase. At present, however, it cannot be differentiated whether the ammonia tunnel is formed immediately upon the binding of PRPP (i.e. in the binary complex) or whether it is fully formed only after ammonia is released upon glutamine hydrolysis (i.e. in the ternary complex).

Asparagine Synthetase

Like GPATase, asparagine synthetase belongs to the Ntn family of glutamine amidotransferases. Other known members of this family include glucosamine 6-phosphate synthase and glutamate synthase (60, 61). Asparagine synthetase B (ASB) from *E. coli* is a bifunctional enzyme that catalyzes the production of asparagine from aspartate, glutamine, and one molecule of ATP (Equation 10).

$$\text{Aspartate} + \text{glutamine} + \text{MgATP} \rightarrow \text{asparagine} + \text{glutamate} + \text{MgADP} \quad 10.$$

As isolated from *E. coli*, the enzyme is a homodimer with each subunit containing 553 amino acid residues. The crystal structure of a site-directed mutant

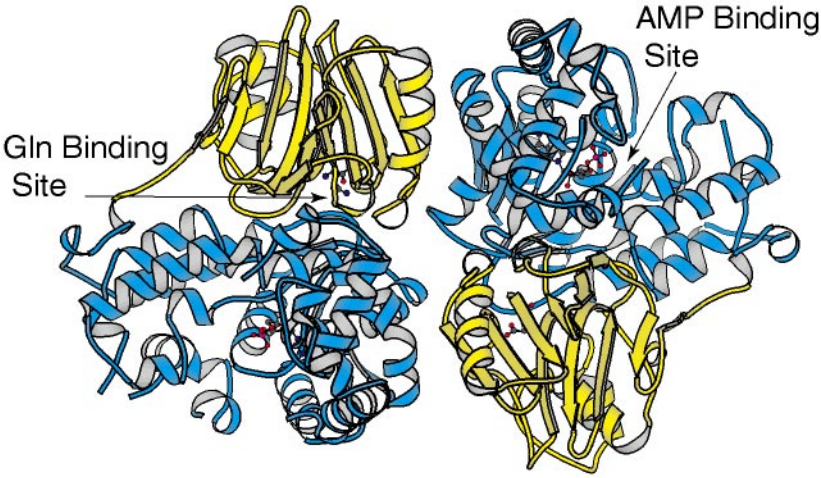

Figure 7 Ribbon representation of the ASB dimer. The molecular dyad of the dimer is oriented perpendicular to the plane of the page. Each subunit of ASB can be divided into the glutaminase domain (yellow) and the synthetase motif (cyan). The subunit:subunit interface is quite extensive, with a buried surface area of ∼2220 Å^2. X-ray coordinates employed for this drawing were obtained from the Protein Data Bank (1CT9).

of the *E. coli* enzyme, namely C1A, was recently solved in the presence of both glutamine and AMP (108). Each subunit folds into two distinct structural motifs defined by Ala-1 to Asp-194 and by Trp-195 to Gly-516, which correspond to the glutaminase and synthetase domains, respectively, as shown in Figure 7. The N-terminal region of ASB is responsible for glutamine hydrolysis, and the C-terminal motif provides the binding pockets for ATP and aspartate and the catalytic machinery required for the subsequent production of the β-aspartyl intermediate and its ultimate reaction with ammonia.

As expected on the basis of amino acid sequence identities, the N-terminal domain of ASB is strikingly similar to that observed for the N-terminal motif of GPATase. Specifically, the α-carbons for the N-terminal domains of these two proteins superimpose with a root-mean-square deviation of 1.4 Å for 176 structurally equivalent residues. Likewise, the C-terminal domain of ASB is similar to that of GMP synthetase: The α-carbons for these two models superimpose with a root-mean-square deviation of 1.9 Å for 79 structurally equivalent residues. In terms of three-dimensional topology, the N-terminal domain of ASB contains two layers of antiparallel β-sheet with each layer containing six strands and the glutamine ligand wedged between these two layers of sheet. The C-terminal synthetase portion of ASB contains a five-stranded parallel β-sheet flanked on either side by α-helices with the AMP moiety lying across the C-terminal edge of the β-sheet. In the X-ray model of the ASB/glutamine/AMP model, the last 37 residues are disordered in both subunits.

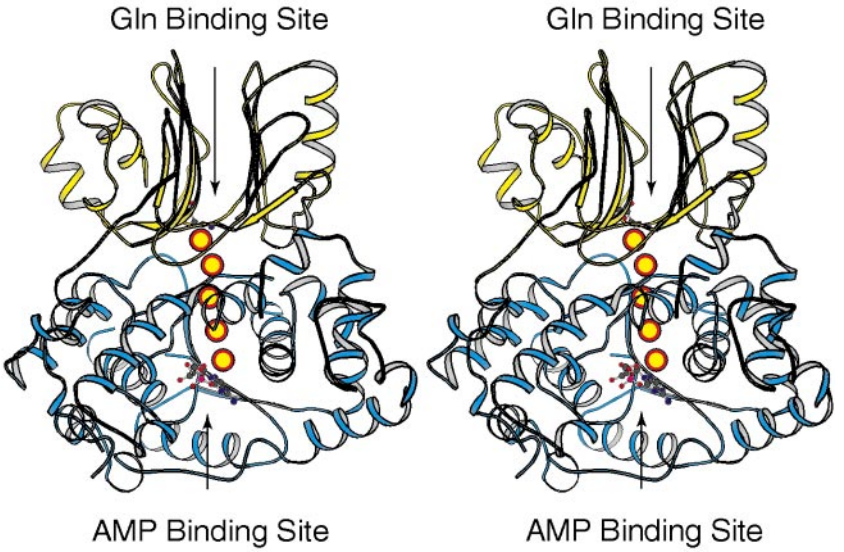

Figure 8 Stereoview of one ASB monomer. A molecular tunnel, as indicated by the yellow spheres, connects the glutamine binding site to the synthetase active site. This tunnel is ~19 Å long.

From this initial structure of ASB, a molecular tunnel of 19 Å connecting the two catalytic sites of the protein was identified as indicated in Figure 8. The walls of this tunnel are composed of backbone atoms and mostly hydrophobic side chains as in GPATase. Unlike GPATase, however, approximately half of these amino acid residues along the molecular tunnel of ASB are not strictly conserved (108). Additional biochemical and structural studies are in progress in several laboratories to more fully define the ammonia tunnel in ASB and the manner in which the two active sites communicate with one another.

Thymidylate Synthase–Dihydrofolate Reductase

Thymidylate synthase (TS) and dihydrofolate reductase (DHFR) catalyze sequential reactions in the de novo biosynthesis of thymidine 5′-monophosphate (dTMP). TS catalyzes the reductive methylation of 2′-deoxyuridine-5′-monophosphate (dUMP) by 5,10-methylene-5,6,7,8-tetrahydrofolate (CH_2-THF) to produce dTMP and 7,8-dihydrofolate (DHF). DHFR catalyzes the subsequent NADPH-dependent reduction of DHF to form 5,6,7,8-tetrahydrofolate (THF). A third enzyme, serine hydroxymethyltransferase, regenerates CH_2-THF to initiate a new round of dTMP synthesis. Both TS and DHFR exist as distinct monofunctional enzymes in bacteriophage, bacteria, fungi, and mammals (109, 110). In protozoa and some higher plants, however, these two activities are found on a bifunctional polypeptide (111–114). In these TS-DHFR complexes, the N-terminal DHFR functionality is

connected to the C-terminal TS domain by a linker peptide. The length of the linker depends on the source of the enzyme. Kinetic evidence for substrate channeling of DHF between the TS and DHFR domains has been reported for the TS-DHFR complex from *Leishmania major* and *Toxoplasma gondii* (115–117). The crystal structure of the *L. major* TS-DHFR complex suggests that this class of enzymes employs a completely different method to channel a reaction intermediate between two distal active sites than the one used by tryptophan synthase and members of the glutamine amidotransferase family (118, 119). Interestingly, an engineered protein, in which a polypeptide linker has been employed to link the monofunctional TS and DHFR from *E. coli*, behaves kinetically the same as a mixture of the two monofunctional enzymes (120).

Kinetic Evidence for DHF Channeling in TS-DHFR Early evidence for substrate channeling using the TS-DHFR complex from *L. major* came from measurements of the time course of $NADP^+$ formation starting from dUMP, CH_2-THF, and NADPH (115). In comparative assays, using a mixture of the monofunctional TS and DHFR enzymes from *Leishmania casei* (*L. casei*), the production of $NADP^+$ displayed a lag when TS was limiting. The overall time course closely matched the one predicted theoretically in a coupled system of two noninteracting enzymes. In parallel experiments with the *L. major* TS-DHFR, no lag period or DHF was detected. Because precision was restricted by a lower detection limit of 12 s, it was concluded that at least 80% of DHF was channeled directly between the active sites of TS-DHFR. A recent isotope dilution experiment that failed to observe an isotope dilution of DHF is also consistent with the direct channeling of DHF (116). Similar results were observed with TS-DHFR from *T. gondii* (117). Additional evidence for substrate channeling in TS-DHFR from *T. gondii* was obtained by a comparative inhibition experiment (117). The DHFR domain of the *T. gondii* TS-DHFR was separately expressed and purified. This domain was shown to have the same DHFR activity as the full-length enzyme. Furthermore, both proteins were similarly inhibited by trimethoprim, a competitive folate analog, when DHF and NADPH were included as substrates. However, when CH_2-THF, dUMP, and NADPH were provided as substrates, it took ~20-fold more trimethoprim to inhibit the DHFR activity of *T. gondii* TS-DHFR than to inhibit to the same extent the DHFR activity of a mixture of *T. gondii* DHFR domain and monofunctional *L. casei* TS. From these results it was inferred that the effective local concentration of DHF at the DHFR site must be 20-fold higher in the bifunctional system than in the monofunctional system, consistent with the channeling of DHF in TS-DHFR.

In a recent study, Liang & Anderson monitored the pre-steady-state time course of the overall reaction catalyzed by *L. major* TS-DHFR (116). In a single turnover experiment, no trace of DHF was detected, and a lag time in the formation of THF was absent. This is very similar to the pre-steady-state time courses observed with tryptophan synthase. The transient kinetic results are fully consistent with the channeling of DHF. Fits to various kinetic models uncovered two critical features of this channeling event (116). First, there must be a substrate channeling step

with a rate constant greater than 1000 s^{-1}. Second, the rate of DHFR catalysis in the overall reaction must be at least one order of magnitude faster than the DHFR partial reaction. The chemical trigger for the activation of DHFR catalysis is thought to be the covalent enzyme intermediate that has been shown to form at the TS site (116). This intermediate can be trapped by using 5-fluoro-2′-deoxyuridine-5′-monophosphate (FdUMP), a dead-end inhibitor of TS (121, 122). Using fluorescence energy transfer by the coenzyme, Liang & Anderson were able to detect the activation of the DHFR site upon the formation of a ternary complex with FdUMP and CH2-THF at the TS site (116). Allosteric signaling of this sort is reminiscent of the situation observed in tryptophan synthase (the aminoacrylate intermediate at the β site) (24) and CPS (the carboxy phosphate intermediate at the first ATP site) (76).

Structural Evidence for Electrostatic Channeling The crystal structure of the *L. major* TS-DHFR was solved in the presence of two pairs of substrate analogs (118). FdUMP and 10-propargyl-5, 8-dideazafolate (PDDF) were bound at the TS site, and methotrexate and NADPH were bound at the DHFR site. Both PDDF and methotrexate are folate analogs, specific for TS and DHFR, respectively. From the crystal structure it is clear that the TS and DHFR activities are embedded in two distinct domains. The folate binding sites of the two domains are separated by approximately 40 Å. No obvious tunnel within the interior of the protein, similar to those found in tryptophan synthase, CPS, GPATase, and ASB, can be located, although the kinetic evidence clearly mandates some form of DHF channeling (115–117). The distribution of an electrostatic potential on TS-DHFR, however, clearly shows a strongly positive electrostatic channel across the surface of the protein that links the TS site to the DHFR site some 40 Å away. DHF has a net charge of -2. Moreover, intracellular folates exist mostly in forms with γ-linked glutamyl moieties (typically 3 to 9) (123). Because each additional glutamyl residue adds an incremental charge of -1, these polyglutamylfolates are highly negatively charged. The binding of polyglutamylfolates to monofunctional TS has been shown to be electrostatic (124, 125). It was therefore proposed that the channeling of DHF in TS-DHFR is achieved through an electrostatic-based mechanism, instead of a tunneling process as observed with tryptophan synthase, CPS, GPATase, and ASB (118). The exact manner in which DHF is transported across this “electrostatic highway” is still not well understood.

Formiminotransferase-Cyclodeaminase

Formiminotransferase-cyclodeaminase (FT-CD) is another bifunctional enzyme that likely transports a reaction intermediate through electrostatic channeling. FT-CD from pig liver is a single polypeptide of molecular weight 62,000, containing an N-terminal FT domain and a C-terminal CD domain (for a review see 126). The FT motif transfers the formimino group of formiminoglutamate to THF, producing 5-formiminotetrahydrofolate (FTHF) and glutamate. The CD domain catalyzes the

cyclization of FTHF to yield 5, 10-methenyltetrahydrofolate and ammonia. Channeling of FTHF is observed only when the substrate has four or more γ-linked glutamyl moieties, with the pentaglutamyl derivative exhibiting optimal channeling efficiency (127). The crystal structure of FT-CD is not available. However, inspection of the structure of the separately expressed FT domain of FT-CD with bound folinic acid, a product analog, reveals an electrostatic channel traversing the width of the FT domain (128). It is likely that a channeling mechanism similar to that suggested for TS-DHFR is operative in this case. It is suspected that electrostatic channeling might well be a general strategy for other bifunctional systems that use polyglutamyl folates as substrates. A review of folate-mediated reactions has been published (129).

2-Oxo Acid Dehydrogenase Complex

The family of 2-oxo acid dehydrogenases contains some of largest known protein complexes and includes pyruvate dehydrogenase, 2-oxo glutarate dehydrogenase, branched-chain 2-oxo acid dehydrogenase, and acetoin dehydrogenase (130). The molecular weights of these macromolecular complexes range between four to ten million daltons. The complexes are composed of multiple copies of three major components: a thiamin diphosphate (ThDP)-dependent 2-oxo acid dehydrogenase, or E1; a dihydrolipoyl acyltransferase, or E2; and a dihydrolipoamide dehydrogenase, or E3. The core of each complex is usually constituted of 24 copies of the E2 catalytic domains in octahedral symmetry or 60 copies in icosahedral symmetry (130–132). The lipoyl domain of E2 is connected to the catalytic core by a linker peptide. Multiple copies of E1 and E3 are stacked onto the E2 core (130). Three cofactors are used during catalysis: ThDP in E1, lipoamide in E2 (formed by covalent attachment of lipoic acid to a lysine residue in the lipoyl domain of E2), and flavin adenine dinucleotide (FAD) in E3. E1 catalyzes the decarboxylation of the substrate to form an acyl-ThDP intermediate and then transfers the acyl group reductively to the lipoamide of E2. The acyl-lipoamide, bound to the lipoyl domain of E2, then visits the catalytic site of E2, where the acyl group is transferred to coenzyme A (CoA) to produce acyl-CoA and reduced lipoamide. The reduced lipoamide finally visits the active site of E3, where it is oxidized by NADH (130, 131).

Kinetic studies indicate that the rate of reductive acylation of lipoamide of E2 by E1 is much higher than that of free lipoyl domains under comparable conditions (131, 133, 134). Modification of the lipoyl domains in some cases completely abolishes the reductive acylation by E1 (135). Recently, the crystal structures of E1, E2, and E3 have been separately solved (136–141). It is apparent that efficient catalysis in the 2-oxo acid dehydrogenase complex is in part due to a totally different kind of substrate channeling: covalent substrate channeling. The structure for E1 of the 2-oxoisovalerate dehydrogenase complex from *Pseudomonas putida* reveals a 20-Å-long funnel-shaped channel leading to the active site of E1 (136). The channel is hydrophobic and appears suitable to accommodate the lipoamide

arm of E2. In a typical tunneling scenario, the enzyme produces a reaction intermediate at one active site, and then channels it to the next active site without exchange with the bulk solvent. 2-Oxo acid dehydrogenase complex uses a different strategy. It instead generates an enzyme-bound intermediate and transfers to the next active site through covalent channeling.

Lumazine Synthase/Riboflavin Synthase Complex

The lumazine synthase/riboflavin synthase complex (LS/RS) from *B. subtilis* is an enzyme complex of one million daltons, consisting of a core of 3 α-subunits and a surrounding icosahedral capsid of 60 β-subunits (for a review see 142). This complex catalyzes the final two steps in the biosynthesis of riboflavin, which produce the precursor of flavin mononucleotide and flavin adenine dinucleotide (143–145). The β-subunit catalyzes a lumazine synthase reaction, the formation of 6,7-dimethyl-8-ribityllumazine (LUM) from 5-amino-6-ribitylamino-2,4(1*H*,*3H*)-pyrimidinedione (PYR) and 3,4-dihydroxy-2-butanone 4-phosphate (DHB). The α-subunit catalyzes a riboflavin synthase reaction, the dismutation of LUM to generate riboflavin, which is the final product, and PYR, which is recycled in the lumazine synthase reaction. The overall reaction stoichiometry catalyzed by the $\alpha_3\beta_{60}$ complex therefore involves the formation of one molecule of riboflavin from one molecule of PYR and two molecules of DHB.

The kinetic behavior of LS/RS in assays with DHB and PYR fits a model of leaky channeling (146). Contrary to a predicted lag in riboflavin formation by a free diffusion model, it was observed that the rate of riboflavin formation reached its maximum value at time $t = 0$ and remained high while LUM accumulated in the reaction solution. When DHB or PYR was depleted, the rate of riboflavin formation was reduced by >30-fold despite the high concentration of the LUM intermediate in the bulk solvent. Apparently, an initial fraction of LUM is directly channeled to the α-site when DHB and PYR are present. After exhaustion of one of the substrates, the enzyme complex uses LUM in the bulk solvent via a dissociative mechanism. Kis & Bacher found that the channeling/diffusion partition ratio depends on substrate concentration and pH (146). The partition ratio approaches unity when both substrates are present at low concentrations.

The crystal structures of the icosahedral β_{60} capsid have been obtained from the native enzyme complex and artifactual β_{60} capsid (147–149). The two structures are nearly identical. The structure of the β-subunit is currently unknown. The β-capsid is an assembly of 12 densely packed pentamers. The 60 identical active sites are located at the interface between adjacent pentamer subunits in close proximity to the inner capsid surface. Five channels run parallel to the five-fold symmetries of the capsid. These channels appear to allow the passage of DHB and PYR but are too narrow for the exit of riboflavin into the bulk solution (148). The structural features for the channeling of LUM to the active site of the trimeric α-core have not yet been identified.

CONCLUDING REMARKS

The use of molecular tunnels for the passage of reaction products from one active site to the next provides a mechanism for the protection of reactive intermediates from the external medium. In enzymes such as tryptophan synthase and carbamoyl phosphate synthetase, the tunnels are apparently formed prior to the binding of individual substrates to the protein. In contrast, the tunnel in glutamine phosphoribosylpyrophosphate amidotransferase does not appear to form until after the binding of both substrates to the two active sites is complete. Molecular tunnels are expected to be found in all of the glutamine amidotransferases where the ammonia formed from the hydrolysis of glutamine is used as a nucleophile in a subsequent chemical reaction. It appears certain that additional types of tunnels will be found for polyfunctional enzymes bearing multiple active sites. In the limited number of examples examined thus far, a significant amount of allosteric communication seems to occur between the active sites connected by the molecular tunnel. This communication provides the conduit for the synchronization of the individual reactions.

ACKNOWLEDGMENTS

Work in our own laboratories on the mechanism for the tunneling of ammonia in carbamoyl phosphate synthetase and asparagine synthetase has been supported in part by the National Institutes of Health (DK30343 to FMR and GM55513 to HMH). We thank Dr. James B Thoden for aid in the figure preparation and for helpful discussions.

LITERATURE CITED

1. Srere PA. 1987. *Annu. Rev. Biochem.* 56:89–124
2. Ovadi J. 1991. *J. Theor. Biol.* 152:1–22
3. Spivey HO, Ovadi J. 1999. *Methods* 19:306–21
4. Anderson KS. 1999. *Methods Enzymol.* 308:111–45
5. Easterby JS. 1981. *Biochem. J.* 199:155–61
6. Westerhoff HV, Welch GR. 1992. *Curr. Top. Cell. Regul.* 33:361–90
7. Rudolph J, Stubbe J. 1995. *Biochemistry* 34:2241–50
8. Ushiroyama T, Fukushima T, Styre JD, Spivey HO. 1992. *Curr. Top. Cell. Regul.* 33:291–307
9. Ovadi J, Huang Y, Spivey HO. 1994. *J. Mol. Recognit.* 7:265–72
10. Dewar MJS, Storch DM. 1985. *Proc. Natl. Acad. Sci. USA* 82:2225–29
11. Wakil SJ, Stoops JK, Joshi VC. 1983. *Annu. Rev. Biochem.* 52:537–79
12. Batke J. 1989. *Trends Biochem. Sci.* 14:481–82
13. Mathews CK, Sinha NK. 1982. *Proc. Natl. Acad. Sci. USA* 79:302–6
14. Ovadi J, Keleti T. 1978. *Eur. J. Biochem.* 85:157–61

15. Welch GR. 1977. *Prog. Biophys. Mol. Biol.* 32:103–91
16. Keleti T, Ovadi J. 1988. *Curr. Top. Cell. Regul.* 29:1–33
17. Vertessy B, Ovadi J. 1987. *Eur. J. Biochem.* 164:655–59
18. Geck MK, Kirsch JF. 1999. *Biochemistry* 38:8032–37
19. Shimamoto N. 1999. *J. Biol. Chem.* 274: 15293–96
20. Jeltsch A, Pingoud A. 1998. *Biochemistry* 37:2160–69
21. Erskine SG, Baldwin GS, Halford SE. 1997. *Biochemistry* 36:7567–76
22. Schurr JM. 1979. *Biophys. Chem.* 9:413–14
23. Wittenberg JB, Wittenberg BA. 1990. *Annu. Rev. Biophys. Chem.* 19:217–41
24. Anderson KS, Miles EW, Johnson KA. 1991. *J. Biol. Chem.* 266:8020–33
25. Liang P-H, Anderson KS. 1998. *Biochemistry* 37:12195–205
26. Miles EW. 1979. *Adv. Enzymol. Relat. Areas Mol. Biol.* 49:127–86
27. Yanofsky C, Crawford IP. 1972. In *The Enzymes*, ed. PD Boyer, 7:1–31. New York: Academic
28. Miles EW. 1991. *Adv. Enzymol. Relat. Areas Mol. Biol.* 64:93–172
29. Miles EW. 1995. In *Subcellular Biochemistry*, ed. BB Biswas, S Roy, 24:207–54. New York: Plenum
30. Pan P, Woehl E, Dunn MF. 1997. *Trends Biochem. Sci.* 22:22–27
31. Matchett WH, DeMoss JA. 1975. *J. Biol. Chem.* 250:2941–46
32. Hutter R, Niederberger P, DeMoss JA. 1986. *Annu. Rev. Microbiol.* 40:55–77
33. Crawford IP. 1989. *Annu. Rev. Microbiol.* 43:567–600
34. Hyde CC, Ahmed SA, Padlan EA, Miles EW, Davies DR. 1988. *J. Biol. Chem.* 263:17857–71
35. Rhee S, Parris KD, Ahmed SA, Miles EW, Davies DR. 1996. *Biochemistry* 35:4211–21
36. Miles EW, Phillips RS, Yeh HJ, Cohen LA. 1986. *Biochemistry* 25:4240–49
37. Rhee S, Parris KD, Hyde CC, Ahmed SA, Miles EW, Davies DR. 1997. *Biochemistry* 36:7664–80
38. Miles EW, Rhee S, Davies DR. 1999. *J. Biol. Chem.* 274:12193–96
39. Brzovic' PS, Ngo K, Dunn MF. 1992. *Biochemistry* 31:3831–39
40. Brzovic' PS, Hyde CC, Miles EW, Dunn MF. 1993. *Biochemistry* 32:10404–13
41. Dunn MF, Aguilar V, Brzovic' PS, Drewe WFJ, Houben KF, et al. 1990. *Biochemistry* 29:8598–607
42. Lane AN, Kirschner K. 1991. *Biochemistry* 30:479–84
43. Creighton TE. 1970. *Eur. J. Biochem.* 13:1–10
44. Yanofsky C, Rachmeler M. 1958. *Biochim. Biophys. Acta* 28:640–41
45. Matchett WH. 1974. *J. Biol Chem.* 249: 4041–49
46. DeMoss JA. 1962. *Biochim. Biophys. Acta* 62:279–93
47. Leja CA, Woehl EU, Dunn MF. 1995. *Biochemistry* 34:6552–61
48. Schlichting I, Yang X-J, Miles EW, Kim AY, Anderson KS. 1994. *J. Biol. Chem.* 269:26591–93
49. Anderson KS, Kim AY, Quillen JM, Sayers E, Yang X-J, Miles EW. 1995. *J. Biol. Chem.* 270:29936–44
50. Kirschner K, Lane AN, Strasser AWM. 1991. *Biochemistry* 30:472–78
51. Houben KF, Dunn MF. 1990. *Biochemistry* 29:2421–29
52. Kawasaki H, Bauerle R, Zon G, Ashmed SA, Miles EW. 1987. *J. Biol. Chem.* 262: 10678–83
53. Strambini GB, Cioni P, Peracchi A, Mozzarelli A. 1992. *Biochemistry* 31:7535–42
54. Brzovic' PS, Saway Y, Hyde CC, Miles EW, Dunn MF. 1992. *J. Biol. Chem.* 267:13028–38
55. Pan P, Dunn MF. 1996. *Biochemistry* 35: 5002–13

56. Anderson PM. 1995. In *Nitrogen Metabolism and Excretion*, ed. PJ Walsh, P Wright, pp. 33–49. New York: CRC Press
57. Jones ME. 1980. *Annu. Rev. Biochem.* 49:253–79
58. Deleted in proof
59. Meister A. 1989. *Adv. Enzymol. Relat. Areas Mol. Biol.* 62:315–746
60. Zalkin H. 1993. *Adv. Enzymol. Relat. Areas Mol. Biol.* 66:203–309
61. Zalkin H. 1998. *Adv. Enzymol. Relat. Areas Mol. Biol.* 72:87–144
62. Anderson PM, Meister A. 1966. *Biochemistry* 5:3164–69
63. Miles BW, Banzon JA, Raushel FM. 1998. *Biochemistry* 37:16773–79
64. Thoden JB, Miran SG, Phillips JC, Howard AJ, Raushel FM, Holden HM. 1998. *Biochemistry* 37:8825–31
65. Lusty CJ. 1992. *FEBS Lett.* 314:135–38
66. Thoden JB, Holden HM, Wesenberg G, Raushel FM, Rayment I. 1997. *Biochemistry* 36:6305–16
66a. Tesmer JJG, Klem JJ, Deras ML, Davisson VJ, Smith JL. 1996. *Nat. Struct. Biol.* 3:74–86
67. Thoden JB, Raushel FM, Benning MM, Rayment I, Holden HM. 1999. *Acta Crystallogr. D* 55:8–24
68. Nyunoya H, Lusty CJ. 1983. *Proc. Natl. Acad. Sci. USA* 80:4629–33
69. Raushel FM, Thoden JB, Holden HM. 1999. *Biochemistry* 38:7891–99
70. Holden HM, Thoden JB, Raushel FM. 1998. *Curr. Opin. Struct. Biol.* 8:679–85
71. Holden HM, Thoden JB, Raushel FM. 1999. *Cell. Mol. Life Sci.* 56:507–22
72. Wimmer MJ, Rose IA, Powers SG, Meister A. 1979. *J. Biol. Chem.* 254:1854–60
73. Raushel FM, Villafranca JJ. 1980. *Biochemistry* 19:3170–74
74. Mullins LS, Lusty CJ, Raushel FM. 1991. *J. Biol. Chem.* 266:8236–43
75. Raushel FM, Villafranca JJ. 1979. *Biochemistry* 18:3424–29
76. Miles BW, Raushel FM. 2000. *Biochemistry* 39:5051–56
77. Huang XY, Raushel FM. 1999. *Biochemistry* 38:15909–14
78. Gibson GE, Mullins LS, Raushel FM. 1998. *Bioorg. Chem.* 26:255–68
79. Rubino SD, Nyunoya H, Lusty CJ. 1986. *J. Biol. Chem.* 261:11320–27
80. Cohen NS, Kyan FS, Jyan SS, Cheung CW, Raijman L. 1985. *Biochem. J.* 229:205–11
81. Wang TT, Bishop SH, Himoe A. 1972. *J. Biol. Chem.* 247:4437–40
82. Mullins LS, Raushel FM. 1999. *J. Am. Chem. Soc.* 121:3803–4
83. Huang XY, Raushel FM. 2000. *Biochemistry* 39:3240–47
84. Huang X, Raushel FM. 2000. *J. Biol. Chem.* 275:26233–40
85. Raushel FM, Mullins LS, Gibson GE. 1998. *Biochemistry* 37:10272–78
86. Deleted in proof
87. Christopherson RI, Jones ME. 1980. *J. Biol. Chem.* 255:11381–95
88. Belkaid M, Penverne B, Herve G. 1988. *Arch. Biochem. Biophys.* 262:171–80
89. Penverne B, Belkaid M, Herve G. 1994. *Arch. Biochem. Biophys.* 309:85–93
90. Irvine HS, Shaw SM, Paton A, Carrey EA. 1997. *Eur. J. Biochem.* 247:1063–73
91. Nakamura J, Straub K, Wu J, Lou L. 1995. *J. Biol. Chem.* 270:23450–55
92. Deleted in proof
93. Brannigan JA, Dodson G, Duggleby HJ, Moody PLE, Smith JL, et al. 1995. *Nature* 378:416–19
94. Messenger LJ, Zalkin H. 1979. *J. Biol. Chem.* 254:3382–92
95. Wong JY, Bernlohr DA, Turnbough CL Jr, Switzer RL. 1981. *Biochemistry* 20:5669–74
96. Switzer RL. 1989. *Biofactors* 2:77–86
97. Bernlohr DA, Switzer RL. 1981. *Biochemistry* 20:5675–81
98. Grandoni JA, Switzer RL, Makaroff CA, Zalkin H. 1989. *J. Biol. Chem.* 264:6058–64

99. Smith JL, Zaluzec EJ, Wery J-P, Niu LW, Switzer RL, et al. 1994. *Science* 264:1427–33
100. Muchmore CRA, Krahn JM, Kim JH, Zalkin H, Smith JL. 1998. *Protein Sci.* 7:39–51
101. Smith JL. 1995. *Biochem. Soc. Trans.* 23:894–98
102. Kim JH, Krahn JM, Tomchick DR, Smith JL, Zalkin H. 1996. *J. Biol. Chem.* 271:15549–57
103. Musick WD. 1981. *Crit. Rev. Biochem.* 11:1–34
104. Krahn JM, Kim JH, Burns MR, Parry RJ, Zalkin H, Smith JL. 1997. *Biochemistry* 36:11061–68
105. Parry RJ, Burns MR, Jiralerspong S, Alemany L. 1997. *Tetrahedron* 53:7077–88
106. Beza AK, Chen S, Smith JL, Zalkin H. 1999. *J. Biol. Chem.* 274:36498–504
107. Chen S, Burgner JW, Krahn JM, Smith JL, Zalkin H. 1999. *Biochemistry* 38:11659–69
108. Larsen TM, Boehlein SK, Schuster SM, Richards NGJ, Thoden JB, et al. 1999. *Biochemistry* 38:16146–57
109. Ackermann WW, Potter VR. 1949. *Proc. Soc. Exp. Biol. Med.* 72:1–9
110. Blakley RL. 1984. In *Chemistry and Biochemistry of Folates*, ed. RL Blakley, SJ Benkovic, 1:191–253. New York: Wiley
111. Feyone R, Roland S. 1980. *Proc. Natl. Acad. Sci. USA* 77:5802–6
112. Ivanetich KM, Santi DV. 1990. *FASEB J.* 4:1591–97
113. Cella R, Carbonera D, Orsi R, Ferri G, Ladarola P. 1991. *Plant Mol. Biol.* 16:975–82
114. Lazar G, Zhang H, Goodman HM. 1993. *Plant J.* 3:657–68
115. Meek TD, Garvey EP, Santi DV. 1985. *Biochemistry* 24:678–86
116. Liang P-H, Anderson KS. 1998. *Biochemistry* 37:12195–205
117. Trujillo M, Donald RGK, Roos DS, Greene PJ, Santi DV. 1996. *Biochemistry* 35:6366–74
118. Knighton DR, Kan C-C, Howland E, Janson CA, Hostomska Z, et al. 1994. *Nat. Struct. Biol.* 1:186–94
119. Stroud RM. 1994. *Nat. Struct. Biol.* 1:131–34
120. Trujillo M, Duncan R, Santi DV. 1997. *Protein Eng.* 10:567–73
121. Moore M, Ashmed F, Dunlap RB. 1986. *Biochemistry* 25:3311–17
122. Santi DV, McHenry CS, Raines RT, Ivanetich KM. 1987. *Biochemistry* 26:8606–22
123. McGuire JJ, Coward JK. 1985. In *Folates and Pterins*, ed. RL Blakley, SJ Benkovic, pp. 135–90. New York: Wiley
124. Kisliuk RL, Gaumont Y. 1974. *J. Biol. Chem.* 249:4100–3
125. Kisliuk RL, Gaumont Y, Baugh CM, Galivan JH, Maley GF, Maley F. 1979. In *Chemistry and Biology of Pteridines*, ed. RL Kisliuk, GM Brown, pp. 431–35. New York: Elsevier/North Holland
126. Shane B, Stokstad ELR. 1984. See Ref. 110, 1:33–55
127. Paquin J, Baugh CM, Mackenzie RE. 1985. *J. Biol. Chem.* 260:14925–31
128. Kohls D, Sulea T, Purisima EO, Mackenzie RE, Vrielink A. 2000. *Structure* 8:35–46
129. Appling DR. 1991. *FASEB J.* 5:2645–51
130. Reed LJ. 1974. *Acc. Chem. Res.* 7:40–46
131. Perham RN. 1991. *Biochemistry* 30: 8501–12
132. Izard T, Aevarsson A, Allen MD, Westphal AH, Perham RN, et al. 1999. *Proc. Natl. Acad. Sci. USA* 96:1240–45
133. Berg A, Westphal AH, Bosma HJ, deKok A. 1998. *Eur. J. Biochem.* 252:45–50
134. Berg A, deKok A. 1997. *Biol. Chem.* 378:617–34
135. Wallis NG, Allen MD, Broadhurst RW, Lessard IA, Perham RN. 1996. *J. Mol. Biol.* 263:463–74
136. Evarsson A, Seger K, Turley S, Sokatch JR, Hol WGJ. 1999. *Nat. Struct. Biol.* 6:785–92

137. Hubner G, Tittmann K, Killenberg-Jabs M, Schaffner J, Spinka M, et al. 1998. *Biochim. Biophys. Acta* 1385:221–28
138. Harris RA, Paxton R, Depaoli-Roach AA. 1982. *J. Biol. Chem.* 257:13915–18
139. Burgi HB, Dunitz JD, Lehn JM, Wipff G. 1974. *Tetrahedron* 30:1563–72
140. Hawes JW, Schnepf RJ, Jenkins AE, Shimomura Y, Popov KM, Harris RA. 1995. *J. Biol. Chem.* 270:31071–76
141. Schellenberger A. 1998. *Biochim. Biophys. Acta* 1385:177–86
142. Bacher A, Eberhardt S, Fischer M, Mortl S, Kis K, et al. 1997. *Methods Enzymol.* 280:389–99
143. Neuberger G, Bacher A. 1986. *Biochem. Biophys. Res. Commun.* 127:175–81
144. Volk R, Bacher A. 1990. *J. Biol. Chem.* 265:19479–85
145. Kis K, Volk R, Bacher A. 1995. *Biochemistry* 34:2883–92
146. Kis K, Bacher A. 1995. *J. Biol. Chem.* 270:16788–95
147. Ladenstein R, Schneider M, Huber R, Bartunik HD, Wilson K, et al. 1988. *J. Mol. Biol.* 203:1045–70
148. Ladenstein R, Ritsert K, Huber R, Richter G, Bacher A. 1994. *Eur. J. Biochem.* 223:1007–17
149. Ritsert K, Huber R, Turk D, Ladenstein R, Schmidt-Base K, Bacher A. 1995. *J. Mol. Biol.* 253:151–67

Annual Review of Biochemistry
Volume 70, 2001

CONTENTS